Astronomy
&
Astrophysics

A new sample of large angular size radio galaxies

II. The optical data

L. Lara[1,⋆], I. Márquez[1,⋆], W. D. Cotton[2], L. Feretti[3], G. Giovannini[3,4], J. M. Marcaide[5], and T. Venturi[3]

[1] Instituto de Astrofísica de Andalucía (CSIC), Apdo. 3004, 18080 Granada, Spain
[2] National Radio Astronomy Observatory, 520 Edgemont Road, Charlottesville, VA 22903-2475, USA
[3] Istituto di Radioastronomia (CNR), via P. Gobetti 101, 40129 Bologna, Italy
[4] Dipartamento di Fisica, Universitá di Bologna, via B. Pichat 6/2, 40127 Bologna, Italy
[5] Departimento de Astronomía, Universitat de València, 46100 Burjassot, Spain

Abstract. We constructed and presented in the first paper of this series a new sample of 84 large angular size radio galaxies by selecting from the NRAO VLA Sky Survey objects with angular size $\geq 4'$, declination above $+60°$ and total flux density at 1.4 GHz ≥ 100 mJy. In this paper we present optical spectra and images of those galaxies associated with the radio emission for which no redshift was known prior to our observations. Optical counterparts have been identified for all (but one) members of the sample. After our observations, a reliable spectroscopic redshift is available for 67 objects (80%) from the sample. This paper, the second of a series of three, contributes to increase the number of well-defined samples of radio galaxies with ample spectroscopic information.

Key words. galaxies: active – galaxies: nuclei – galaxies: distances and redshift – radio continuum: galaxies

1. Introduction

Lara et al. (2001), hereafter Paper I, presented a new sample of large angular size radio galaxies selected from the NRAO[1] VLA[2] Sky Survey (NVSS; Condon et al. 1998). The sample, covering a sky area of π steradians, was constructed under the following selection criteria: declination above $+60°$, total flux density at 1.4 GHz greater than 100 mJy and angular size larger than $4'$. 122 radio sources were pre-selected and observed with the VLA with higher angular resolution at 1.4 and 4.9 GHz for confirmation, and a total of 84 radio galaxies were selected for the final sample (see Table 2 in Paper I). In Paper I we have shown that, within the selection criteria, our sample is homogeneous and suitable for statistical studies. Moreover, our sample represents a substantial increase in the number of known giant radio galaxies (GRGs; defined as those

with a projected linear size[3] ≥ 1 Mpc), with 22 new objects belonging to this class. This sample, together with other new samples currently being studied by other groups (Schoenmakers et al. 2000, 2001; Machalski et al. 2001) raises the number of known GRGs to above one hundred.

The identification of the optical counterpart of the radio core emission, and the determination of its redshift, is a necessary step for the study of any sample of radio galaxies. In our case, many of the members of the sample were poorly known, both at radio and optical wavelengths. First, a reliable optical identification of the radio galaxies had not been possible previous to our work since only low angular resolution radio data existed and, consequently, only a poor determination of the radio core position was possible. The radio maps of the sample members presented in Paper I allowed us to obtain accurate positions of the core components (see Table 2) and, in most cases, to attempt successful identification of the associated galaxy on the Digital Sky Survey (DSS). Second, only 35% of the galaxies in the sample had measured redshifts. Thus, it was necessary to tackle the task of measuring the redshift of all the remaining galaxies in order to obtain useful physical parameters for a subsequent study.

⋆ Visiting Astronomer, German-Spanish Astronomical Center, Calar Alto, operated by the Max-Planck-Institut für Astronomie jointly with the Spanish National Commission for Astronomy.

[1] National Radio Astronomy Observatory.

[2] Very Large Array, operated by the NRAO.

---

[3] We assume that $H_0 = 50$ km s^{-1} Mpc^{-1} and $q_0 = 0.5$.

We present here (Paper II) images obtained with the 2.2 m telescope in Calar Alto of the optical counterparts of the sample galaxies for which no redshift was available in the literature at the time of the observations. We have made long-slit spectroscopy of these objects and determined the redshift for 46 (6 uncertain) of them. In the forthcoming third paper of this series, we will present a global analysis of the sample properties.

2. Optical imaging and spectroscopy

We made optical observations of 57 radio galaxies from the sample, pointing the 2.2 m telescope in Calar Alto (Spain) to the position of the radio core component. The log of the observing runs is given in Table 1. We used the Calar Alto Faint Object Spectrograph (CAFOS) equipped with a SITe-1d 2048×2048 CCD. CAFOS allows direct imaging and spectroscopy, with a spatial scale of $0\rlap{.}''53$ per pixel with this CCD. To obtain the spectra, we used a medium resolution grism (200 Å/mm), sensitive to the wavelength range of 4000 to 8500 Å, that provides a spectral resolution of 4.47 Å/pixel.

The standard procedure followed during the observations was to take first one 300 s exposure image in the Johnson R-band in order to identify the optical host of the radio galaxy core component, whose position had already been accurately determined from VLA radio observations (Paper I) and registered on the DSS plates. Once the galaxy coincident with the radio core was located in the image, we obtained a spectrum with the CAFOS long-slit configuration, taking two equal exposures (usually 900 s, or 1200 s for weaker objects) to be added in order to reject the cosmic rays. We used a $2''$ wide slit placed north-south, except on J1220+636, J1251+756, J0819+756 and J1251+787, for which a $-45°$ slit rotation was applied in order to avoid contamination from nearby bright stars. Some objects required longer exposures in the R-band in order to detect the associated optical galaxy, and in some of the weaker galaxies, although detected, we did not attempt to obtain a spectrum.

The data reduction and calibration were performed following standard procedures with the IRAF[4] software, involving dark and flat field corrections. Wavelength calibration was carried out using exposures of mercury-helium-rubidium arc lamps taken just before or after the target exposure. No flux calibration of the spectra was attempted since the atmospheric conditions were far from photometric during most of the observing nights. In fact, some of the resulting spectra have quite a low signal to noise ratio due to bad weather conditions (e.g. J0757+826 or J0828+632). Examining the intensity profile along the slit on each spectrum, we determined the most adequate

---

[4] IRAF is the Image Reduction and Analysis Facility made available to the astronomical community by the National Optical Astronomy Observatories, which are operated by the Association of Universities for Research in Astronomy (AURA), Inc., under contract with the U.S. National Science Foundation.

Table 1. Optical observations.

Nights	Average seeing ($''$)	σ	Code[a]
Sep. 26th 1997	1.88	0.36	a1
Oct. 30th 1998	1.98	0.33	b1
Oct. 31st 1998	1.16	0.14	b2
Nov. 1st 1998	1.23	0.17	b3
Nov. 2nd 1998	1.72	0.22	b4
Dec. 8th 1998	1.08	0.17	c1
Dec. 9th 1998	1.02	0.14	c2

[a] Code used in Table 2 to indicate the epoch of observation of each source.

region for the determination and subtraction of the sky contribution, and the region centered on the target galaxy which we summed in order to create the corresponding 1-dimension spectrum.

Images of the optical counterpart of the observed radio galaxies and their spectra are shown in Fig. 1. The average seeing ($FWHM$) determined for each night using foreground stars in the different R-band images is displayed in Table 1, and varies from $2''$ on the night of 30th October 1998 to $1''$ on 9th December 1998. Two prominent atmospheric absorption bands at $\lambda = 7604$ Å and $\lambda = 6882$ Å, corresponding to the Fraunhofer A and B bands of molecular oxygen, are marked with vertical lines on the spectra in Fig. 1.

3. Notes on singular sources

In this section we make a brief description of those observed galaxies which show some type of remarkable properties in the optical regime (luminosity, spectrum or nearby environment), when compared with the rest of the sample:

J0342+636: A spheroidal galaxy with a prominent broad Hα emission line. A weaker broad Hβ line and [OIII] narrow emission lines are also detected. J0342+636 presents a close companion at an angular distance of $6.8''$ in position angle (PA) of $-53°$, which corresponds to a linear projected distance of 20.5 kpc (if both galaxies are assumed to be at the same redshift).

J0455+603: At the time of the optical observations we had not correctly identified the core component in the radio structure, and consequently did not find the associated galaxy after two exposures of 300 s each. The core component of J0455+603 was misidentified with a bright and compact feature in our 1.4 GHz VLA map (see Paper I). However, we have now identified the core with a weaker component with flat spectrum at $16''$ in NW direction from the previously assumed core, which is coincident with the galaxy marked in Fig. 1. Coordinates in Table 2 have been corrected with respect to those listed in Paper I.

J0502+670: The host galaxy of this Fanaroff-Riley type I radio source (FR I; Fanaroff & Riley 1974) is a bright elliptical at $z = 0.085$ with an spectrum characterized by the presence of stellar absorption features. It has
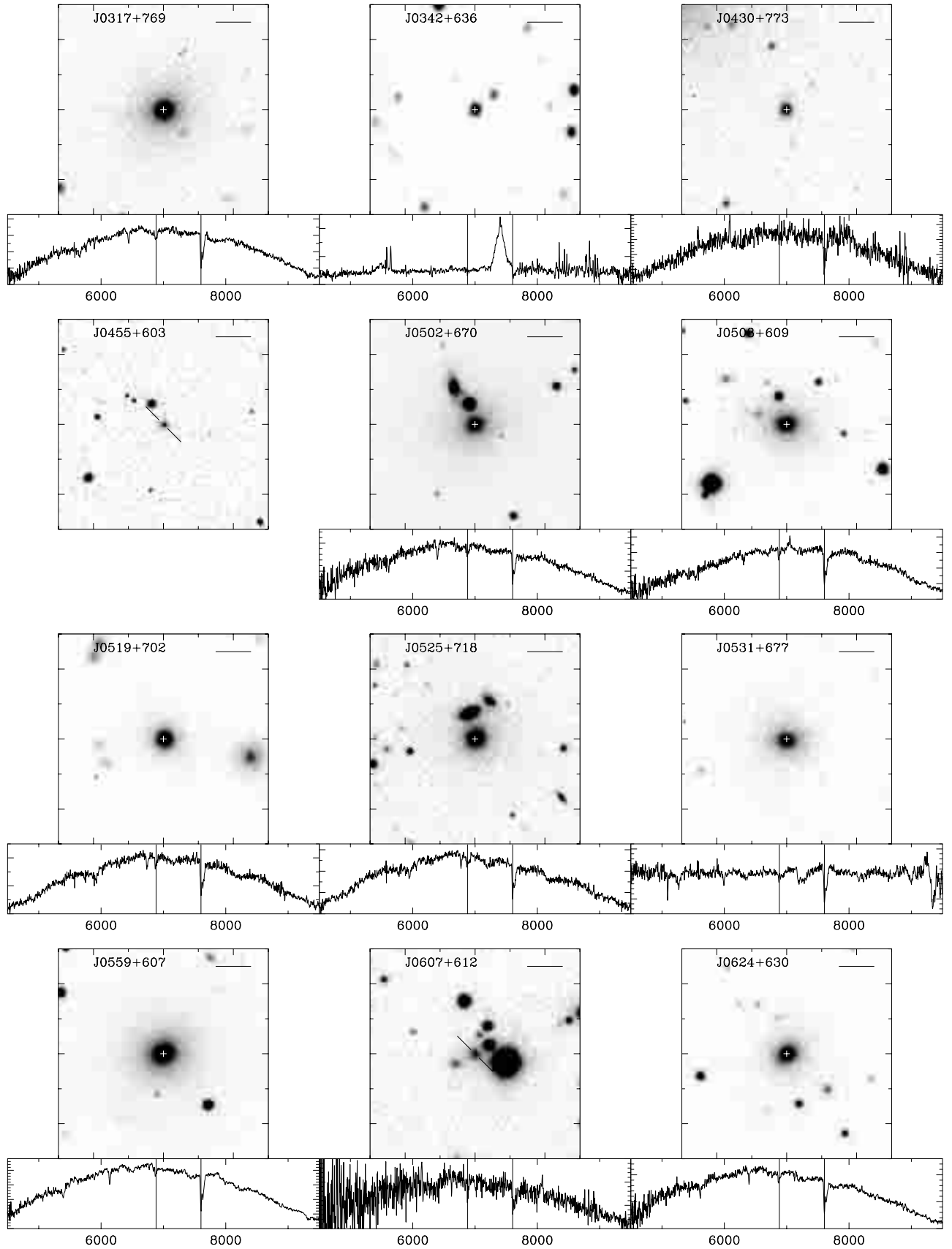
Fig. 1. Optical images of the galaxies identified with the radio sources of the sample. The white cross (or broken line) helps to identify the galaxy coincident with the position of the radio core. The segment on upper right corresponds to an angular size of 10″. Below each image we display the optical spectrum, obtained with a long slit of 2″ width. Flux units are arbitrary and wavelengths are given in Å. The two vertical solid lines mark the position of atmospheric absorption bands produced by O_2.
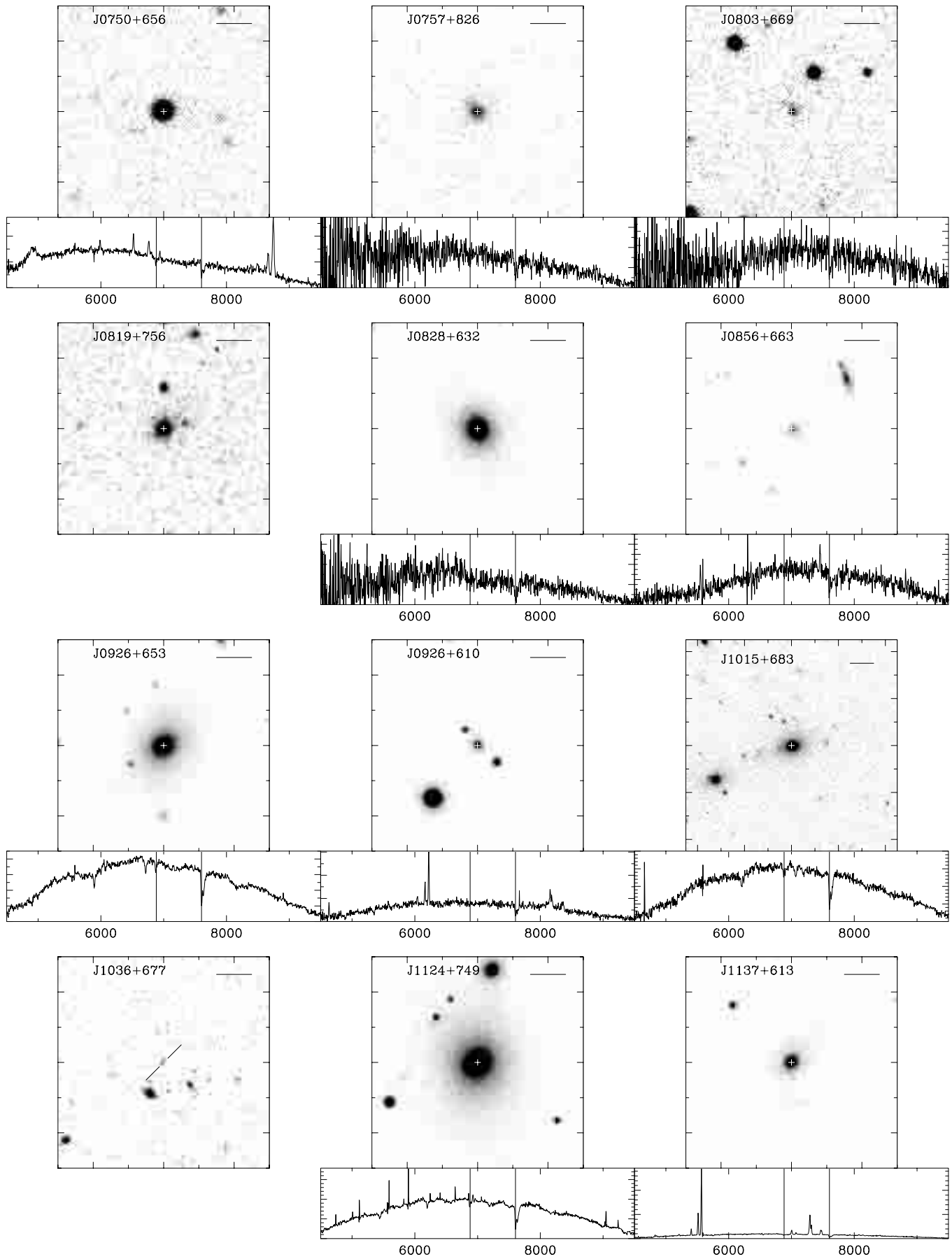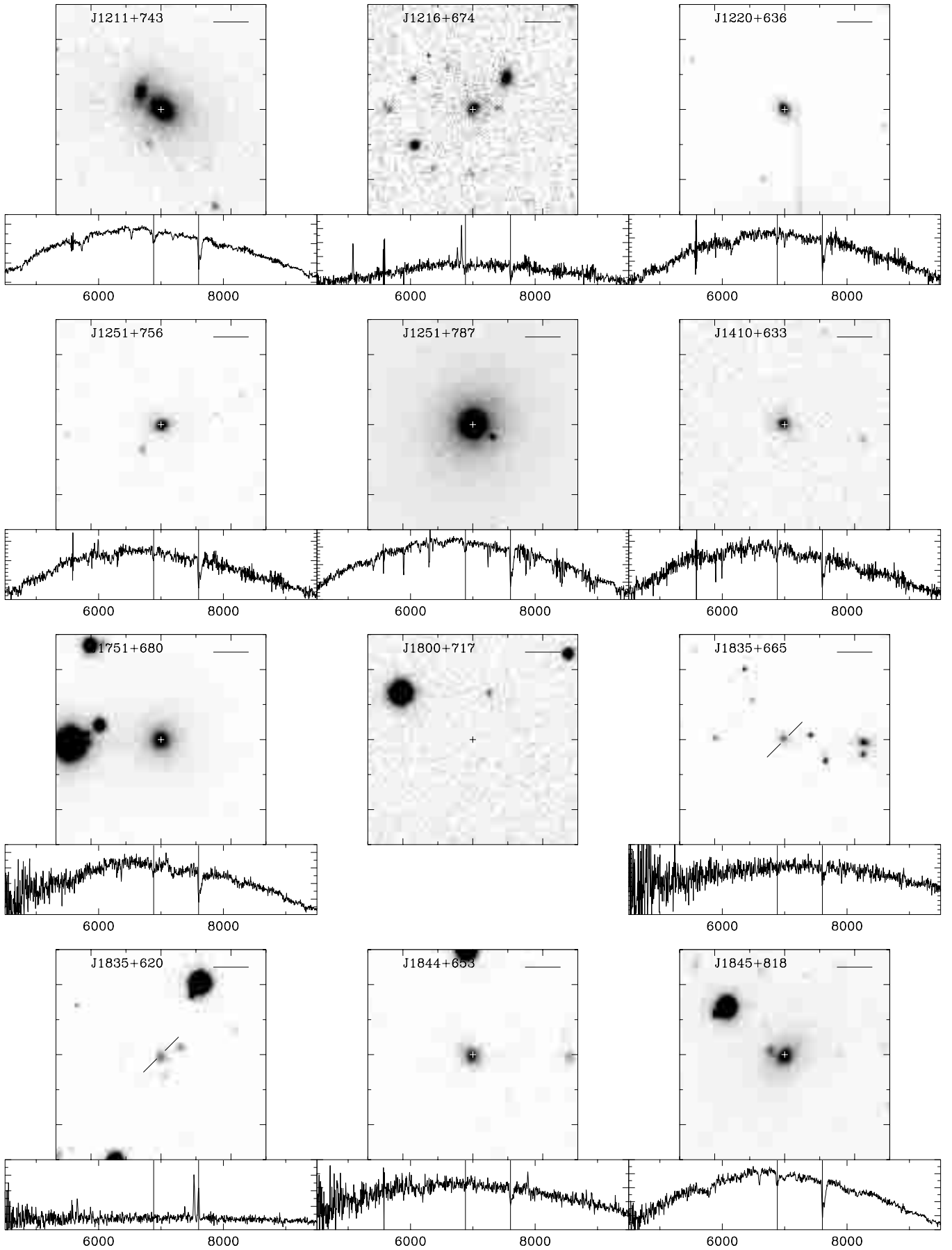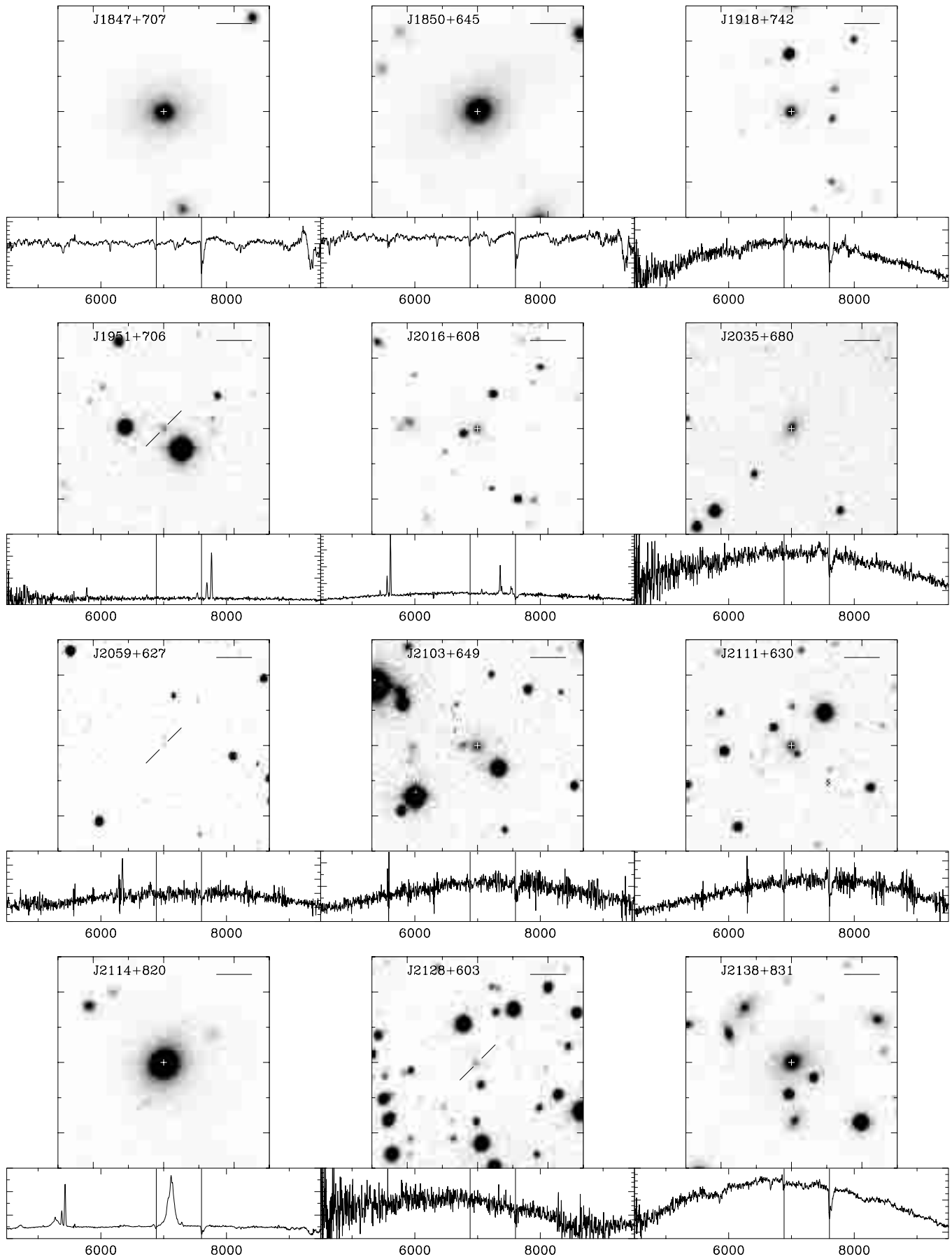
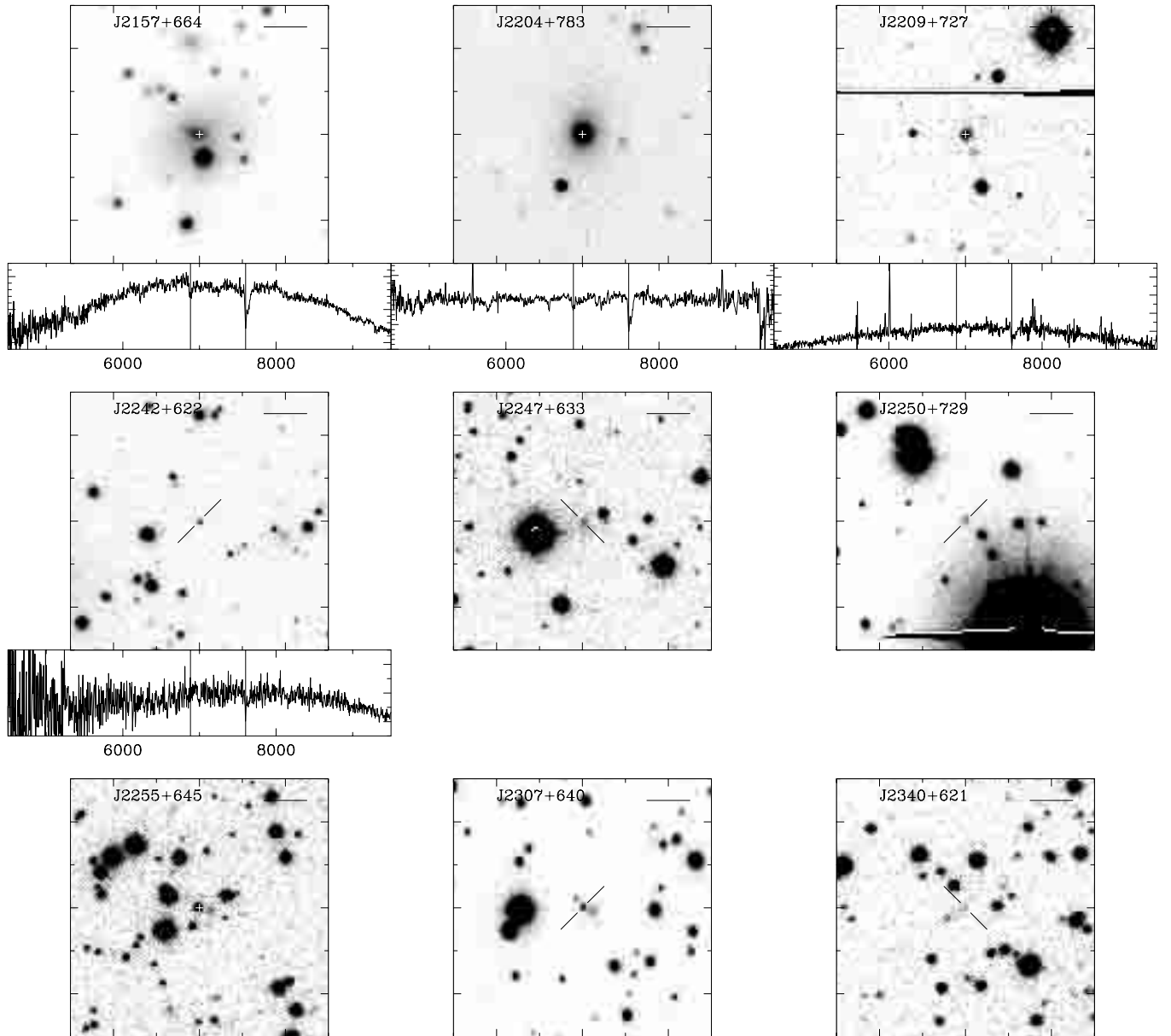Fig. 1. continued.

Fig. 1. continued.

Fig. 1. continued.

Fig. 1. continued.

a close companion separated by 12″ at PA of 29°, which corresponds to 25.7 kpc if assumed to be at the same redshift. There is a foreground star ($m_R \sim 13$) between the two galaxies.

J0525+718: A bright elliptical galaxy is the source of this low power radio galaxy. There are two nearby galaxies at 7.6″ in PA +2° and at 12″ in PA −21°, which if assumed to be at the same redshift of J0525+718 correspond to projected distances of 26 and 41 kpc, respectively.

J0750+656: The most distant radio source in our sample, at $z = 0.747$. It is optically identified with a 16.4 magnitude quasar type object.

J1015+683: Two galaxies in the field can be identified with components in the complex radio structure of this source (see Fig. 2), which confirms that J1015+683 results from the superposition of two distinct radio galaxies
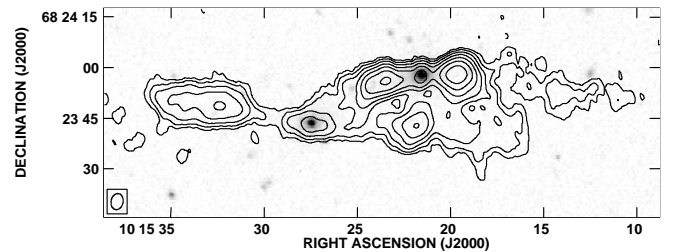

Fig. 2. Superposition of a radio image of J1015+683 at 4.9 GHz (Paper I) with the Johnson R-band filter optical image of the same field.

with their main axes in a similar (projected) direction. The angular distance of the two galaxies is 35.4″, which at the redshift of the northern one ($z = 0.199$) corresponds to 149 kpc. The classification of this radio galaxy as a giant

(Paper I) must be postponed until a redshift determination of the southern galaxy.

J1137+613: This radio galaxy, of Fanaroff-Riley type II (FR II), originates from an spheroidal galaxy. Its spectrum presents high signal to noise ratio emission lines (Hβ, [OIII], [OI], Hα, [NII], [SII]).

J1211+743: The radio emission originates from a bright elliptical galaxy. It has a nearby companion at $7.5''$ in PA $+51°$, which corresponds to 19.5 kpc if assumed to be at the same redshift of J1211+743. There are no emission features in the spectrum, which is dominated by the continuum and some stellar absorption lines.

J1800+717: This is the only object in our sample for which no hint of the optical counterpart of the radio emission is found. The cross in Fig. 1 represents the position of the radio core of this FR II radio galaxy. We made three 300 s exposures on the field centered at this position but nothing was detected. The R-band extinction is only of 0.1 magnitudes in this region (Schlegel et al. 1998), so the associated galaxy must either be very distant or intrinsically weak. A limit to its apparent magnitude ($m_R > 19.5$) can be estimated from the magnitude of a weak object located $13''$ northward from the radio core position.

J1845+818: It is identified with an elliptical galaxy. At a distance of $4.4''$ in PA $+76°$ from the galaxy center, there is a small, possibly elongated feature. It is coincident with the direction of the radio jet, although if it is related to the jet is not clear. Most probably, it is a small galaxy close to the radio emitting elliptical galaxy, at a projected distance of 12.5 kpc if assumed to be at the same redshift. The galaxy spectrum presents only stellar absorption lines.

J2059+627: We obtained only a bad quality optical image of this field, although sufficient to identify a very weak feature associated with the radio core. Two 1200 s long-slit exposures revealed a weak continuum with prominent [OIII] emission lines.

J2114+820: A peculiar low power radio galaxy of FR I type associated with an elliptical galaxy which shows prominent broad Hα, Hβ and Hγ emission lines, and narrow [OIII] lines (Lara et al. 1999). The galaxy has a bright compact core associated to the nuclear activity.

J2138+831: The origin of this radio source is a bright elliptical galaxy residing in the cluster Abell 2387. Its spectrum shows no emission lines, being characterized by stellar absorption lines.

J2157+664: We made three 300 s exposures on this galaxy which revealed an extended elliptical galaxy with an apparent double core in east-west direction. The radio core is coincident with the western feature. No emission lines are found in the spectrum. The galaxy, with a galactic latitude of $+9.2°$, lies in a crowded field, with possibly smaller galaxies around, and a bright foreground star located nearby southwards.

J2247+633: We made two 300 s exposures on the field centered at the radio core position, and found a very weak feature coincident with the radio core. The galactic latitude of this galaxy is only of $+3.7°$. We did not attempt to obtain the spectrum of this galaxy.

J2250+729: We made three 300 s exposures on the field centered at the radio galaxy core. A very weak feature associated with the radio core was found, close to a bright star with apparent $m_R = 10.1$. The galactic latitude of this galaxy is $+12.1°$. We did not attempt to obtain the spectrum of this galaxy.

J2340+621: We made two 300 s exposures and tentatively found the optical counterpart of this radio galaxy in a crowded star field. The galactic latitude is only $+0.4°$ and the R-band extinction in this region is of 4.0 magnitudes (Schlegel et al. 1998). We did not attempt to obtain the optical spectrum of this galaxy.

4. Results

In Table 2 we present the main results derived from the observations reported in this paper:

Column 1: IAU source name at epoch J2000.

Columns 2, 3: right ascension and declination (J2000).

Column 4: galactic latitude.

Column 5: code defined in Table 1 indicating the epoch of observation.

Column 6: integration time for the spectroscopic observations.

Column 7: redshift derived from our observations or from the literature.

Column 8: notes about the optical spectrum: SEL – strong emission lines present; WEL – weak emission lines; AbL – absorption lines only.

Column 9: apparent photographic magnitudes derived from the red band Palomar survey (DSS R-band). Magnitudes of faint galaxies (above the 16th magnitude) have been obtained from the USNO-A2.0 catalogue (Monet et al. 1998), and compared with the APM catalogue (http://www.ast.cam.ac.uk/~apmcat). In general, we found good agreement between these two catalogues, but we adopted the mean value in the few cases where the discrepancy was larger than 0.4 magnitudes. When USNO-A2.0 did not provide information on a requested galaxy, we adopted the APM magnitude. The magnitudes of brighter galaxies (up to the 16th magnitude) have been determined directly from the DSS using the available photometric calibration (Doggett et al. 1996). However, we note that the apparent magnitudes of the brighter extended galaxies are subject of large errors (sometimes larger than 3 magnitudes) probably due to the non-linear behavior of the photographic plates.

Column 10: effective radius of the galaxies derived by fitting a $r^{1/4}$ profile to the brightness distribution. Although the low sensitivity or quality of some galaxy images prevented us from obtaining reasonable fits for them, in all possible cases the profile was consistent with that typical of elliptical galaxies.

Column 11: type of radio structure: I and II stand for FR I and FR II type radio galaxies, respectively. Distinction between the two classes is based solely on morphological

Table 2. Sample of large angular size radio galaxies from the NVSS survey.

Name	RA (J2000.0) (^{h} ^{m} ^{s})	Dec (J2000.0) ($^\circ$ $'$ $''$)	b ($^\circ$)	Epoch	T_{exp} (s)	z	Notes	m_R (mag)	r_e (kpc)	Radio Type
J0109+731	01 09 44.265	73 11 57.17	10.4			0.181^a	SEL	—	—	II
J0153+712	01 53 25.786	71 15 06.53	9.0			0.022^a	SEL	10.4	—	I
J0317+769	03 17 54.061	76 58 37.82	16.5	b1	2×900	0.094	AbL	14.7	37.0	I
J0318+684	03 18 19.026	68 29 32.08	9.4			0.090^b	WEL	17.5	—	II
J0342+636	03 42 10.148	63 39 33.73	6.8	a1	2×900	0.128	SEL	17.9	—	II
J0430+773	04 30 49.490	77 22 58.44	19.5	b1	2×1200	0.215	WEL	18.5	10.4	II
J0455+603	04 55 45.847	60 23 48.94	10.6	c1		—	—	—	—	I
J0502+670	05 02 54.732	67 02 30.15	15.2	b2	2×1200	0.085	AbL	13.9	28.9	I
J0508+609	05 08 27.258	60 56 27.48	12.2	b2	2×900	0.071	WEL	14.6	34.6	I
J0519+702	05 19 17.132	70 13 48.68	18.1	b1	2×900	0.144	AbL	16.1	33.1	I
J0525+718	05 25 27.094	71 52 39.25	19.4	b2	2×900	0.150	AbL	15.9	26.8	I
J0531+677	05 31 25.925	67 43 50.23	17.9	a1	2×900	0.017	AbL	8.8	3.0	I
J0546+633	05 46 24.622	63 21 32.50	17.2			0.049^a	??	10.9	—	I
J0559+607	05 59 38.690	60 44 00.96	17.5	b2	2×900	0.042	AbL	12.6	14.3	I
J0607+612	06 07 34.919	61 14 43.52	18.6	b3	2×1200	0.227	WEL	—	—	I/II
J0624+630	06 24 29.063	63 04 02.50	21.1	b3	2×900	0.085	AbL	14.5	10.4	I
J0633+721	06 33 40.842	72 09 24.92	24.4			0.090^b	AbL	15.0	—	I/II
J0654+733	06 54 26.525	73 19 50.36	26.1			0.115^b	SEL	15.2	—	II
J0750+656	07 50 34.425	65 41 25.50	30.6	b1	2×900	0.747	SEL	16.4	—	II-QSS
J0757+826	07 57 35.172	82 39 40.86	29.0	b4	3×1200	0.087? (0.06)	AbL	12.0	9.6	I
J0803+669	08 03 45.829	66 56 11.39	31.9	b3	2×1200	0.247? (0.37)	AbL	19.3	—	II
J0807+740	08 07 10.070	74 00 41.58	31.2			0.120^b	SEL	15.8	—	I
J0819+756	08 19 50.504	75 38 39.53	31.7	c2	1×900	0.232^b	SEL	17.7	24.8	II
J0825+693	08 25 59.770	69 20 38.59	33.5			0.538^a	SEL	—	—	II
J0828+632	08 28 56.363	63 13 45.05	34.9	b4	2×1200	— (0.09)	—	13.7	(10.7)	I/II
J0856+663	08 56 16.260	66 21 26.50	37.1	b3	2×1200	0.489	WEL	19.7	—	II
J0926+653	09 26 00.822	65 19 22.88	40.3	b2	2×900	0.140	AbL	15.0	42.3	I
J0926+610	09 26 53.408	61 00 24.87	42.0	b2	1×900	0.243	SEL	17.2	25.8	I
J0939+740	09 39 46.833	74 05 30.78	37.0			0.122^b	AbL	14.8	—	I
J0949+732	09 49 46.157	73 14 23.82	38.1			0.058^a	SEL	12.8	—	II
J1015+683	10 15 21.620	68 23 58.24	42.7	c1	2×900	0.199	AbL	15.1	31.6	?
J1036+677	10 36 41.237	67 47 53.44	44.6	c1		—	—	—	—	II
J1124+749	11 24 47.045	74 55 45.31	40.9	c1	1×900	0.052	WEL	10.7	34.9	I
J1137+613	11 37 21.289	61 20 01.88	53.6	c1	2×900	0.111	SEL	16.2	18.8	II
J1211+743	12 11 58.710	74 19 04.12	42.5	c1	2×900	0.107	AbL	12.6	49.1	I/II
J1216+674	12 16 37.239	67 24 41.97	49.4	c2	2×900	0.362	SEL	18.7	41.0	II
J1220+636	12 20 36.477	63 41 43.82	53.1	c2	2×900	0.188	AbL	15.7	—	II
J1247+673	12 47 33.319	67 23 16.34	49.7			0.107^a	AbL	14.7	—	II
J1251+756	12 51 05.977	75 37 38.94	41.5	c2	2×900	0.197	WEL	16.4	6.9	II
J1251+787	12 51 23.839	78 42 36.29	38.4	c2	900+700	0.045	AbL	10.4	17.1	I
J1313+696	13 13 58.878	69 37 18.74	47.4			0.106^a	SEL	16.0	—	II
J1410+633	14 10 30.609	63 19 00.55	51.6	c1	2×900	0.158	AbL	17.2	13.4	II

^{a} Redshift taken from the NASA Extragalactic Database.
^{b} Redshift from Schoenmakers et al. (1999).

aspects. Those radio galaxies with a difficult distinction between the FR I or FR II types are labelled as I/II.

We plot in Fig. 3 a histogram of the apparent R-band magnitude of the galaxies in the sample. The magnitude distribution is very extended, ranging from 8.2 up to magnitude 19.7 with a peak lying between the 15th and 16th magnitudes. The distribution presents a tail towards brighter objects induced by the poor calibration of photographic plates due to their non-linear behavior. At the other extreme the distribution is influenced by the limiting sensitivity of the DSS ($m_R \leq 20$).

In Fig. 4 we represent the apparent de-reddened R-band magnitude as a function of redshift for the sample members, excepting the three quasar type objects in the sample. We have also added in this plot the radio galaxies (excepting quasars) from the sample constructed by Schoenmakers et al. (2001), who provide a photometry
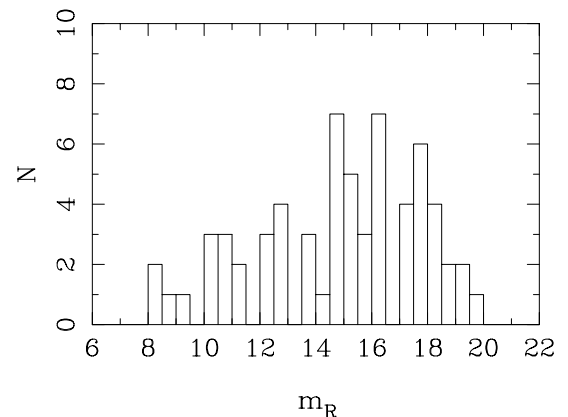

Fig. 3. Histogram of the apparent R-band magnitudes of the galaxies in our sample. The bin size is 0.5 magnitudes.

consistent with ours. We find a relation of the form (least squares fitting)

$$m_R - A(R) = (8.83 \pm 0.35)\log z + (22.96 \pm 0.37) \qquad (1)$$

Table 2. continued.

Name	RA (J2000.0) (h m s)	Dec (J2000.0) (° ′ ″)	b (°)	Epoch	$T_{\exp}$ (s)	z	Notes	m_R (mag)	r_e (kpc)	Radio Type
J1504+689	15 04 12.781	68 56 12.75	43.9			0.318^a	SEL	16.2	—	II-QSS
J1523+636	15 23 45.900	63 39 23.78	46.0			0.204^a	SEL	16.0	—	II
J1530+824	15 30 56.110	82 27 21.02	32.8			0.021^a	??	9.1	—	I
J1536+843	15 36 57.335	84 23 10.42	31.3			0.201^b	WEL	18.2	—	II
J1557+706	15 57 30.190	70 41 20.79	39.3			0.026^a	AbL	8.2	—	I
J1632+825	16 32 31.630	82 32 16.28	31.2			0.023^a	SEL	8.4	—	I
J1650+815	16 50 58.686	81 34 28.11	31.1			0.038^a	??	11.3	—	I
J1732+714	17 32 33.001	71 24 10.50	31.9			0.059^a	??	12.0	—	I
J1733+707	17 33 12.525	70 46 30.36	31.9			0.041^a	??	11.4	—	I
J1743+712	17 43 17.681	71 12 53.98	31.0			— (0.25)	—	17.8	—	II
J1745+712	17 45 43.573	71 15 48.55	30.8			0.216^a	SEL	18.4	—	II
J1751+680	17 51 19.629	68 04 43.05	30.6	b4	2×900	0.079	AbL	12.4	43.6	I
J1754+626	17 54 50.310	62 38 41.96	30.3			0.028^a	WEL	10.3	—	I
J1800+717	18 00 42.622	71 44 41.99	29.6	b4		— ($\geq$0.40)	—	$\geq$19.5	—	II
J1835+665	18 35 07.338	66 35 00.02	26.3	b3	2×1200	0.354? (0.34)	AbL	19.0	14.6	II
J1835+620	18 35 10.405	62 04 07.42	25.6	b1	2×1200	0.518	SEL	—	—	II
J1844+653	18 44 07.443	65 22 03.07	25.2	b1	2×1200	0.197	AbL	17.1	—	II
J1845+818	18 45 15.836	81 49 30.98	27.0	b1	2×900	0.119	AbL	14.3	30.6	II
J1847+707	18 47 34.912	70 44 00.64	25.8	a1	500+900	0.043	AbL	10.6	13.4	I
J1850+645	18 50 45.871	64 30 24.68	24.4	a1	2×900	0.080	AbL	12.6	21.6	I
J1853+800	18 53 52.077	80 02 50.46	26.6			0.214^a	??	17.8	—	II
J1918+742	19 18 34.885	74 15 05.05	24.2	b2	2×1200	0.194	WEL	17.5	8.2	II
J1951+706	19 51 40.825	70 37 39.99	20.7	b3	2×1200	0.550	SEL	—	—	II
J2016+608	20 16 18.630	60 53 57.49	14.0	c1	2×900	0.121	SEL	18.2	10.6	II
J2035+680	20 35 16.549	68 05 41.60	16.1	b2	2×1200	0.133	WEL	18.0	9.9	I
J2042+751	20 42 37.180	75 08 02.52	19.5			0.104^a	SEL	14.7	—	II-QSS
J2059+627	20 59 09.560	62 47 44.11	11.0	c2	2×1200	0.267	SEL	—	—	II?
J2103+649	21 03 13.868	64 56 55.26	12.0	c2	2×1200	0.215	AbL	—	—	II
J2111+630	21 11 20.268	63 00 06.17	10.1	c1	2×900	—	—	—	—	II
J2114+820	21 14 01.179	82 04 48.28	22.3	a1	2×900	0.085	SEL	13.5	—	I
J2128+603	21 28 02.634	60 21 07.96	6.8	b2	2×1200	0.072?	AbL	—	—	II
J2138+831	21 38 42.266	83 06 49.21	22.4	b2	2×900	0.135	WEL	14.5	36.9	I/II
J2145+819	21 45 29.887	81 54 54.22	21.4			0.146^b	SEL	17.1	—	II
J2157+664	21 57 02.572	66 26 10.24	9.2	b3	2×900	0.057?	AbL	—	—	I/II
J2204+783	22 04 09.225	78 22 46.92	18.2	a1	2×900	0.115	AbL	15.1	15.5	II
J2209+727	22 09 33.780	72 45 58.36	13.6	c2	2×1200	0.201	WEL	—	—	II
J2242+622	22 42 32.133	62 12 17.53	3.0	c1	2×1200	0.188?	AbL	—	—	II
J2247+633	22 47 29.714	63 21 15.55	3.7	c2		—	—	—	—	I
J2250+729	22 50 43.621	72 56 16.19	12.1	c1		—	—	—	—	II
J2255+645	22 55 29.943	64 30 06.86	4.4	c2		—	—	—	—	II
J2307+640	23 07 58.533	64 01 39.22	3.4	c2		—	—	—	—	II
J2340+621	23 40 56.435	62 10 45.09	0.4	b3		—	—	—	—	I

^{a} Redshift taken from the NASA Extragalactic Database.
^{b} Redshift from Schoenmakers (1999).

with a correlation coefficient $r = 0.942$ and rms = 1.01 mag. It allows us to estimate, with a typical error of $\sim$30%, the redshift of those galaxies with known magnitudes for which an spectroscopic determination was not possible (values shown in parenthesis in Table 2). For those galaxies with an uncertain spectroscopic redshift, a "photometric" estimation is also provided when possible (shown in parenthesis).

The fact that such a tight correlation between apparent magnitude and redshift exists is an indication that the host galaxies of the sample members have quite similar properties and that a possible orientation dependent beaming of the core emission does not play a significant role as expected for AGNs with their main axis oriented close to the plane of the sky, contrary to favorably oriented objects like blazars.

5. Conclusions

We have made optical observations pointing at the core position of 57 radio galaxies from our sample and in all cases, except one, we have detected the optical galaxy responsible of the radio emission. Even the galaxy J2340+621, at the very low galactic latitude of +0.4° has been tentatively detected. The observed galaxies have profiles consistent with being elliptical. We took spectra of 48 galaxies, of which the redshift could be determined with high confidence for 40 of them and with uncertainty for 6 galaxies. For only 2 galaxies, J0828+632 and J2111+630, we were unable to determine the redshift. However, a "photometric" redshift can be estimated from a correlation derived between apparent magnitudes and spectroscopic redshift of the sample members.
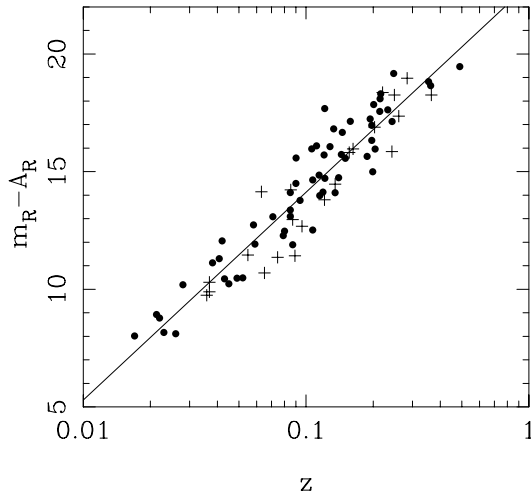
Fig. 4. De-reddened apparent *R*-band magnitudes of the members of our sample (dots) and Schoenmakers' et al. sample (crosses), plotted against their redshifts. The solid line represents a linear fit to the data.

Regarding the properties of the optical spectrum, 36% of the galaxies present spectra with prominent emission lines, 19% of the galaxies show weak emission lines with respect to the continuum emission, and 45% of the galaxies have spectra characterized by stellar absorption lines only.

The fact that our sample is designed to select radio galaxies with their main axes oriented on the plane of the sky is consistent with the spectroscopic results, since only 3 galaxies (J0342+636, J0750+656 and J2114+820) out of 48 observed present broad emission lines, as expected for objects oriented towards the observer according to current unification schemes (e.g. Antonucci 1993).

In a forthcoming paper of this series, we will discuss the possible relations between the different parameters derived from the radio and optical observations presented in this paper and in Paper I, and the possible dependencies of these parameters with the type of radio structure.

References

Antonucci, R. 1993, ARA&A, 31, 473

Condon, J. J., Cotton, W. D., Greisen, E. W., et al. 1998, AJ, 115, 1693

Doggett, J., Postman, M., Lasker, B. M., & Meakes, M. 1996, in Astronomical Data Analysis Software and Systems V, ed. H. George, J. Barnes, & J. Barnes, ASP Conf. Ser., 101, 159

Fanaroff, B. L., & Riley, J. M. 1974, MNRAS, 167, 31

Lara, L., Cotton, W. D., Feretti, L., et al. 2001, A&A, 370, 409, Paper I

Lara, L., Márquez, I., Cotton, W. D., et al. 1999, NewAR, 43, 643

Machalski, J., Jamrozy, M., & Zola, S. 2001, A&A, 371, 445

Monet, D., Bird, A., Canzian, B., et al. 1998, U.S. Naval Observatory Flagstaff Station and Universities Space Research Association stationed at USNOFS

Schlegel, D. J., Finkbeiner, D. P., & Davis, M. 1998, ApJ, 500, 525

Schoenmakers, A. P. 1999, Ph.D. Thesis, University of Utrecht

Schoenmakers, A. P., Mack, K.-H., de Bruyn, A. G., et al. 2000, A&AS, 146, 293

Schoenmakers, A. P., de Bruyn, A. G., Röttgering, H. J. A., & van der Laan, H. 2001, A&A, 374, 861